Kinetics of Soot Oxidation by NO_2

MANISH SHRIVASTAVA,[†] ANH NGUYEN,[‡,§] ZHONGQING ZHENG,[‡,§] HAO-WEI WU,[‡,§] AND HEEJUNG S. JUNG*[,‡,§]

Pacific Northwest National Laboratory, Richland, Washington 99352, Bourns College of Engineering, Center for Environmental Research and Technology (CE-CERT), University of California, Riverside, California 92521, and Department of Mechanical Engineering, University of California, Riverside, California 92521

Received December 4, 2009. Revised manuscript received April 22, 2010. Accepted April 23, 2010.

Modern technologies use NO_2 to promote low-temperature soot oxidation for diesel particulate filter regeneration. In this study, the online aerosol technique of high-temperature oxidation tandem differential mobility analysis is used to study kinetics of soot oxidation by NO_2. Soot particles are exposed to varying temperature and NO_2 mixing ratio inside the furnace resulting from thermal decomposition of NO_2 to NO. This causes soot oxidation rates to vary throughout the furnace. Variations in temperatures and NO_2 mixing ratio are thoroughly accounted for the first time. Soot oxidation rates are calculated as a function of frequency factor A_{soot}, activation energy E_{soot}, and concentration of NO_2 within the furnace at temperatures ranging from 500 to 950 °C. Results suggest A_{soot} and E_{soot} values for soot oxidation of 2.4×10^{-14} (nm $K^{-0.5}$ s^{-1} cm^3 $molecule^{-1}$) and 47.1 kJ mol^{-1}, respectively, when reaction order to NO_2 is assumed as unity. The activation energy for soot oxidation with NO_2 is significantly lower than oxidation with air. However, parts per million levels of NO_2 cause soot oxidation at low temperatures suggesting NO_2 is a stronger oxidant than O_2.

1. Introduction

Soot has a controlling influence on earth's temperature and climate. In addition, soot particles pose significant human health risk. Elimination of soot particle emissions from diesel engines has attracted lots of attention because of potential health risk around urban areas.

Soot particles could be reduced either by modifying the combustion process inside the engine or by removing particles from the exhaust stream. Particles are removed from the exhaust stream using a diesel particulate filter (DPF), followed by catalytic soot oxidation to regenerate the filter (*1*). For these reasons, it is of immense interest to understand the kinetics of soot oxidation in the presence of oxidants like NO_2 and O_2 at temperatures relevant to both in-cylinder and exhaust after-treatment conditions. The high temperature (>800 °C) soot oxidation studies are relevant to modeling soot oxidation inside an engine cylinder or at flame conditions, while the low temperature (300−700 °C) soot oxidation studies are useful in understanding soot oxidation in the diesel exhaust and after-treatment systems such as diesel particulate filters (DPF) (*2*). Regeneration of DPF is performed at low temperatures (300−450 °C) to avoid thermal fatigue of the devices and to minimize energy used for regeneration.

Although there are other oxidants present during diesel soot combustion, a majority of soot oxidation studies were done under oxygen environment or air (*2*−*5*). Stanmore et al. (*6*) reviewed soot oxidation by NO_x (NO_2, NO, and N_2O). They reported the magnitude of soot oxidation reaction rates are in the order of $NO_2 > N_2O \approx NO \approx O_2$, showing NO_2 oxidation most prominent. NO_2 is a stronger oxidant than O_2 promoting low temperature oxidation of soot in the range of 200−500 °C (*7*). NO_2 has also been postulated to have a synergistic role with O_2 in the combustion of diesel soot (*7, 8*). Typically, NO_2 is 5−15% of the total NO_x (less than 50 ppm) in the diesel exhaust. However, oxidation catalysts like Pt could oxidize NO to NO_2 increasing NO_2 mixing ratio to 50% of the total NO_x, in the temperature range of 300−350 °C (*7, 9*). The continuously regenerating trap (CRT) (*10*) in diesel exhaust after-treatment system combines two chemical processes: platinum catalyzed oxidation of NO to NO_2 and oxidation of trapped soot in the presence of NO_2. Thus, it is of interest to better understand kinetics of soot oxidation in the presence of NO_2.

Most of the previous research studied soot oxidation using offline methods such as thermo-gravimetric analysis (TGA) (*8, 11, 12*). However, this method is subject to mass and heat transfer effects that make the quantification of kinetics of soot oxidation difficult. Bulk sample of soot particles is packed by unknown packing ratio. A reasonable decoupling for mass transfer effect is achieved by measuring diffusion coefficient through the bulk sample (*13*). However authors are not aware of good methods to decouple heat transfer effect from bulk sample. The best experimental approach was to put quartz chips in the bulk sample and assume the temperature is uniform (*14*). The advantage of current TDMA (Tandem Differential Mobility Analyzer) method is to determine reaction rate by looking at size change of primary particles decoupling mass and heat transfer effects to begin with.

Higgins et al. (*3, 4*) studied kinetics of soot oxidation from ethylene diffusion flame and from exhaust stream of medium-duty diesel engine over the temperature range of 800−1000 °C in the presence of air as an oxidant. They used the online aerosol technique of high-temperature oxidation tandem differential mobility analysis (HTO-TDMA). This technique offers several advantages over previous offline methods, such as thermogravimetric analysis (TGA) (*8, 11, 12*). The HTO-TDMA method minimizes effects of transport and soot aging (*5*). Choo et al. (*15*) derived oxidation characteristics of spark-discharge generated soot in the presence of NO_2 using the HTO-TDMA method. However, they made significant errors in their analysis, which will be discussed in detail at the discussion section.

In this work, kinetics of soot oxidation using NO_2 as the primary oxidant are investigated using the HTO-TDMA method (*3*−*5*), at furnace temperatures ranging 500−950 °C. NO_2 inlet mixing ratios are varied from 0−600 ppm using N_2 as a carrier gas. A complication in using HTO-TDMA method to study soot oxidation with NO_2 using N_2 as a carrier gas is that NO_2 mixing ratios are not uniform throughout the heated length of the furnace. NO_2 decomposes to NO under N_2 environment inside the tube furnace at temperatures exceeding 500 °C under experimental conditions of this study. NO_2 decomposition in the tube at higher temperatures is modeled using a second order kinetic rate equation. This allows calculation of NO_2 concentration at each axial location throughout the heated length of the furnace. It is noteworthy

* Corresponding author e-mail: heejung@engr.ucr.edu.
[†] Pacific Northwest National Laboratory.
[‡] Bourns College of Engineering, Center for Environmental Research and Technology (CE-CERT).
[§] Department of Mechanical Engineering, University of California.

10.1021/es903672y

Published on Web 05/21/2010

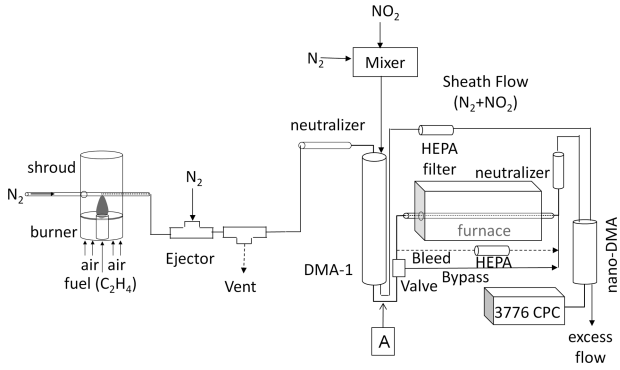

FIGURE 1. Schematic of the experimental system.

that NO_2 concentration depends on thermal expansion of the heated gas within the tube in addition to thermal decomposition of NO_2, while NO_2 mixing ratio (mole fraction in ppm) is independent of thermal expansion and changes only caused by thermal decomposition of NO_2. The kinetic parameters for soot oxidation are derived as a function of nonuniform NO_2 concentrations and temperature in the furnace. The derived kinetic parameters are compared to other studies and implications for future research are discussed.

2. Experimental Method

Polydisperse soot particles are generated by a diffusion flame burner using ethylene as fuel. Particles are sampled through a 1 mm orifice drilled at the bottom of a horizontal 11 mm inner diameter stainless steel sampling tube. Soot particles are diluted and quenched by a constant flow of 5 liters per minute (Lpm) of N_2 through the sampling probe. Secondary dilution of the aerosol flow is done using an ejector dilutor (Air-Vac TD-110H vacuum transducer pump) with N_2 flow of about 20 Lpm at 30 psi as shown in Figure 1. Soot particles are sent to differential mobility analyzer DMA-1 (TSI 3081 series long column DMA) for size selection based on electrical mobility. Size-selected monodisperse soot particles from the first DMA are then oxidized in a high temperature flow reactor and the resulting particle size distribution is measured using the second DMA with a condensation particle counter (CPC) as the detector. The second DMA is a nano-DMA (TSI 3085 series nano-DMA) designed to reduce particle losses of nanoparticle and improve size resolution in the range 3−50 nm (*16*). As shown in Figure 1, a parallel line bypassing the furnace is used to periodically monitor the size and concentration of monodisperse particle stream from DMA-1 at the beginning of each measurement. The bypass line ensures that flame conditions, and particle sizing from DMA-1 are constant throughout the experiment. Our setup is modification of those of Higgins et al. (*3*) and Nienow et al. (*5*) specifically for NO_2 experiment.

Different mixing ratios of the oxidant NO_2 are introduced into the sheath flow of DMA-1 with N_2 as the carrier gas. HEPA filtered excess line from DMA-1 is used as the sheath for DMA-2. A critical orifice is used to maintain 10 Lpm sheath flow for DMA-2 and corresponding excess flow from DMA-1. The monodisperse aerosol flow from DMA-1 is controlled at 1 Lpm using laminar flow element. A 1/2 in. stainless steel tubing with 7 coils (coil diameter of 4 in.) is used to mix N_2 (purity 99.999% Praxair) and base NO_2 gas (certified at 5049 ppm) in different proportions to get desired mixing ratio of NO_2 ranging 0−600 ppm. NO_2 from sheath flow mixes with the particle flow line in DMA-1. Calculations indicate complete mixing for sheath and aerosol flow rates of 10 and 1 Lpm, respectively. NO_2 mixing ratios measured in the monodisperse aerosol line at location marked A in Figure 1 are found to be in agreement with the NO_2 mixing ratios in the excess flow from DMA-1. During the actual experiments, NO_2 mixing ratios in the sheath line are constantly monitored to avoid disturbing the aerosol flow.

Monodisperse particles of 40 nm selected by the first DMA are oxidized in a quartz flow tube placed at the center of a heated furnace (LINDBERG/BLUE M Model HTF55122A). The total length of the furnace is 21 in. (53.3 cm), and the heated length is 12 in. (30.5 cm). The quartz tube (1.2 cm o.d. × 1 cm i.d. × 74 cm long) is surrounded by a 23.5 in. long alumina tube (2.54 cm o.d. × 1.91 cm i.d.) placed inside the furnace. The purpose of the alumina tube is to provide a uniform heat flux to the quartz tube (*3*).

Oxidation of soot particles is studied at different NO_2 mixing ratios and varying furnace set-point temperatures ranging 500−950 °C. TEM images of soot nanoparticles from ethylene diffusion flame in a previous study showed roughly spherical particle shape in the size range 30−60 nm (*5*). The 40 nm particle size is chosen to ensure that particles are roughly spherical as this simplifies the kinetic analysis (*5*), and this is also the smallest size selection from Higgins et al. (*3*) for comparison. Jung (*17*) found that soot oxidation rates became size independent after correcting for density and shape effects for particles in the size range 40−130 nm. Choosing particles of size smaller than 40 nm resulted in loss of sensitivity of measurements at higher temperatures and NO_2 mixing ratios. Also, measurements of soot oxidation at 1 Lpm flow rate showed small decrease in particle diameter as a function of NO_2 mixing ratios and furnace set-point temperatures. The flow rate of 1 Lpm is governed by the ratio of sheath to aerosol flow rates of 10:1. To increase the sensitivity of the method, the gas flow rate through the furnace is reduced to 0.5 Lpm to allow additional residence time for soot oxidation within the furnace, keeping the aerosol flow rate through the DMA constant at 1 Lpm. This is done by bleeding 50% of the flow coming from DMA-1 bypassing the furnace as shown by the dotted line in Figure 1 and then mixing the HEPA filtered bleed flow with the main flow exiting the furnace.

3. Modeling

Higgins et al. (*3*) fitted kinetic parameters in terms of observed decrease of peak particle size in the furnace from size distributions measured by the TDMA, using a nonlinear least-squares fit to experimental data. Using CFD simulations, Shrivastava et al. (*18*) showed that decrease in peak particle diameter was independent of diffusion and thermophoretic effects and served as a reliable parameter to derive soot oxidation rate within the furnace. Decrease in particle diameter is empirically described using a modified form of Arrhenius expression to account for variable NO_2 concentrations within the furnace following Stanmore et al. (*2*) given as:

$$\dot{D}_p = -A_{soot} T^{1/2} \exp\left(-\frac{E_{soot}}{RT}\right)[NO_2]^n \qquad (1)$$

where $\dot{D}_p$ is the rate of decrease of particle diameter with time, A_{soot} is frequency factor, E_{soot} is activation energy, R is the universal gas constant, T and $[NO_2]$ are the absolute furnace temperature in K and the concentration of NO_2 in molecules cm^{-3}, respectively, at any given axial location with the furnace, and n is the reaction order of soot with respect to NO_2. The exponent of temperature is held fixed at 0.5 to roughly account for dependence of collision frequency on temperature (*3*). The reaction order n should be experimentally determined. Various authors reported the reaction order for oxidation of soot with NO_2 as unity ($n = 1$) (*12, 19*). In the present study, the reaction order could not be determined experimentally as soot is subjected to changing

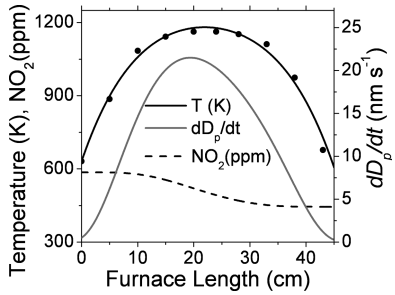

FIGURE 2. Variation of temperature, NO_2 mixing ratio, and soot oxidation rate within the furnace at furnace set-point temperature of 850 °C and inlet NO_2 mixing ratio of 600 ppm. Furnace temperatures are represented by a 4th-order polynomial fit (shown by the solid dark line) to measurements represented by closed circles.

NO_2 concentrations in the furnace. Hence, the reaction order is assumed to be 1 consistent with other studies.

The total decrease in particle size by oxidation in the furnace is found by integrating eq 2 along the furnace length

$$\Delta D_{\mathrm{p}} = \int_0^X \frac{\dot{D}_p(x)}{u(x)}\mathrm{d}x \tag{2}$$

where x is horizontal position in the tube, X is length of the tube, and $u(x)$ is the flow velocity which varies linearly with temperature along the tube length.

Temperatures are measured using a K-type thermocouple at different furnace set-point temperatures as described by Higgins et al. (*3*) at gas flow rate of 0.5 Lpm. Figure 2 shows the measured temperature profile at furnace set-point temperatures of 850 °C. A fourth-order polynomial fit to measurements is used to describe the axial temperature profile throughout the furnace. As shown in Figure 2, temperature is maximum near the middle of the furnace and decreases to room temperature near the inlet and exit of the furnace.

NO_2 balanced in N_2 as a carrier gas is used. At temperatures higher than 500 °C, NO_2 decomposes to NO as a function of temperature and residence time within the furnace. The thermal decomposition of NO_2 is described by the following equation:

$$\mathrm{NO_2 + NO_2 \rightarrow O_2 + NO + NO} \tag{3}$$

The rate expression $k(T)$ for eq 3 is defined as:

$$k(T) = A_{\mathrm{NO_2}} \exp\left(-\frac{E_{\mathrm{NO_2}}}{RT}\right) \tag{4}$$

$k(T)$ is the second-order rate constant in $\mathrm{cm^3\ molecule^{-1}\ s^{-1}}$, $A_{\mathrm{NO_2}}$ is the frequency factor, and $E_{\mathrm{NO_2}}$ is the activation energy.

At any axial location within the furnace, the values of NO_2 concentration could be calculated as function of time and temperature using eqs 4 and 5 given as:

$$\frac{1}{N_t} = 2k(T)t + \frac{1}{N_0} \tag{5}$$

where N_t is the NO_2 concentration (molecules $\mathrm{cm^{-3}}$) at given axial location, t is the time in seconds spent by particles up to that location, and N_0 is the inlet concentration of NO_2 to the furnace at time zero.

Values of $A_{\mathrm{NO_2}}$ and $E_{\mathrm{NO_2}}$ for eq 4 have been experimentally determined by Park et al. (*20*). In this study, NO_2 decomposition within the furnace is measured at different temperatures ranging from 500 to 950 °C at inlet NO_2 mixing ratios of 200 and 600 ppm. Measurements are compared to

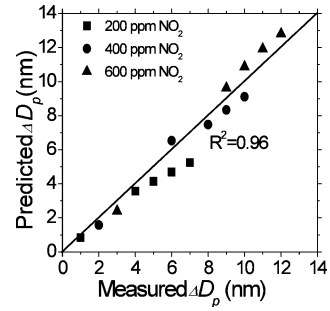

FIGURE 3. Comparison of measured and predicted values showing goodness of fit for change of particle diameter within the furnace.

predicted NO_2 decomposition within the furnace using eq 4 and 5 and value of $E_{\mathrm{NO_2}}$ (116 kJ $\mathrm{mol^{-1}}$) suggested by Park et al. (*20*). The value of $A_{\mathrm{NO_2}}$ used in eq 4 is found by fitting to ten measurements of NO_2 decomposition in the furnace. The fitted $A_{\mathrm{NO_2}}$ (1.59×10^{-11} $\mathrm{cm^3\ molecule^{-1}\ s^{-1}}$) is a factor of 2 higher than corresponding value from Park et al. (*20*) (7.49×10^{-12} $\mathrm{cm^3\ molecule^{-1}\ s^{-1}}$), but within expected range of uncertainty of $A_{\mathrm{NO_2}}$ (*20*). Figure 2 shows the calculated NO_2 mixing ratios throughout the heated length of the furnace using eqs 4 and 5. As shown in Figure 2, NO_2 mixing ratio decreases at high temperature in the furnace. It is noteworthy that influence of radial temperature distribution and resulting NO_2 decomposition on soot oxidation is not considered in the present analysis. Our previous study using comprehensive Computational Fluid Dynamics modeling (*18*) showed that limitations in measurement of accurate radial gas temperature profile in the laminar flow reactor may cause a factor of 2 uncertainty in derived soot oxidation rates. This uncertainty is mainly reflected in value of frequency factor, but does not affect the activation energy for soot oxidation. More accurate analysis would require CFD analysis similar to our previous study, but is beyond the scope of this work.

Soot particles are exposed to nonuniform temperature and oxidant (NO_2) mixing ratios in the furnace. Assuming a reaction order of 1, values of A_{soot} and E_{soot} in eq 1 were first determined by fitting to 15 different values of measured ΔD_{p} at varying furnace set-point temperatures (500−950 °C) and inlet NO_2 mixing ratios (200−600 ppm). Figure 3 shows the quality of fits to measured decrease in particle diameter (ΔD_{p}). Figure 2 also shows the varying soot oxidation rates ($\mathrm{d}D_{\mathrm{p}}/\mathrm{d}t$) on the right-hand y-axis, calculated from the fits. As shown in Figure 2, the instantaneous soot oxidation rate varies throughout the heated length of furnace as function of temperature and NO_2 mixing ratio. The modeling approach described above systematically accounts for varying soot oxidation rates within the furnace.

4. Results

Figure 4 shows representative TDMA scans from the nano-DMA for particles of initial size 40 nm. Figure 4a shows that particle size distribution shifts to smaller sizes with increasing inlet NO_2 mixing ratio at constant furnace set-point temperature of 800 °C. Figure 4b shows decrease of particle sizes at constant inlet NO_2 mixing ratio of 400 ppm and increasing furnace temperatures. Thus particles shrink because of oxidation with both increasing temperatures and increasing oxidant levels. The broadening of particle size distribution with oxidation is because of particles experiencing a range of residence times within the reactor. The varying residence time distribution of particles is because of near-laminar gas flow, buoyancy-induced secondary flows at higher furnace temperatures, and effects of thermophoresis (*18*). Following previous works (*3*−*5*), the results in this study were analyzed with respect to $\Delta D_{\mathrm{p}}/\Delta t$, where ΔD_{p} is the change in peak

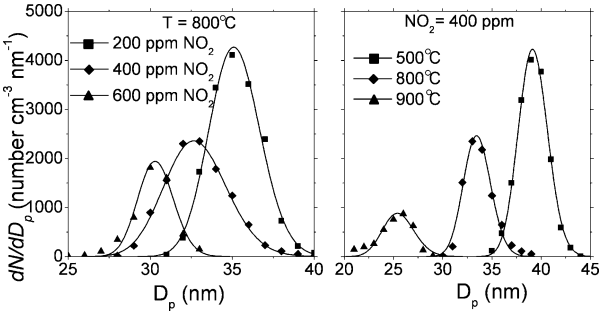

FIGURE 4. TDMA data showing particle number size distribution data (dN/dD_p) for oxidation of 40 nm soot particles at (a) varying inlet NO_2 mixing ratios at furnace set-point temperature of 800 °C and (b) varying furnace set-point temperatures and constant inlet NO_2 mixing ratio of 400 ppm. Points represent measurements, while solid lines are fits to data.

mobility diameter and Δt is the characteristic residence time within the reactor.

Table 1 shows the measured ΔD_p values at different temperatures and inlet NO_2 mixing ratios within the furnace. Interestingly, particles show modest size reduction even at zero NO_2 mixing ratios when nitrogen is the carrier gas at higher furnace temperatures. For example at 950 °C, the decrease in peak mobility diameter under nitrogen environment is 8 nm. Nienow et al. (*5*) observed a size reduction of 4.3 nm at 975 °C for soot particles of initial size 30 nm from ethylene diffusion flame. However, Nienow et al. (*5*) used an aerosol flow rate of 1 Lpm through the same tube geometry as the present study; hence, particle residence times were shorter as compared to the present study. The 40 nm particles are near-spherical, so effects of thermally induced restructuring of aggregates at high temperatures is less likely (*5*). In this work, the soot particles are found to have significant organic carbon content (OC) in addition to elemental carbon (EC). A thermal-optical analysis on the polydisperse soot particles collected on a quartz filter from the flame indicated that OC could be up to 40% of the total carbon (TC). This measurement includes artifacts (including gas phase organics in addition to particle phase). Most of the semivolatile OC would evaporate because of further dilution in the DMA-1 and at furnace temperatures below 500 °C and would not contribute to soot oxidation under experimental conditions in this study. However, some organics, such as PAHs, may be strongly adsorbed on the soot particles. It is plausible that evaporation of strongly adsorbed relatively nonvolatile OC and decomposition of oxygen containing functional groups (*21, 22*) could be responsible for size reduction observed under N_2 environment without NO_2 consistent with conclusion of Nienow et al. (*5*).

To derive oxidative kinetics of soot oxidation, it is necessary to separate the nonoxidative size reduction from calculations of ΔD_p. Following Nienow et al. (*5*), it is assumed that the oxidative and nonoxidative components of ΔD_p are additive. Hence, the oxidative component of ΔD_p is derived by subtracting the ΔD_p measured under N_2 environment from total ΔD_p measured at any given NO_2 mixing ratio as shown in Table 1. Choo et al. (*15*) derived oxidation rate parameters without accounting for the nonoxidative component of ΔD_p, hence their results may be biased.

TABLE 2. Fitted Kinetic Parameters for Soot Oxidation with NO_2

parameter	value
A_{soot} (nm $K^{-0.5}$ s^{-1} cm^3 $molecule^{-1}$)	2.4×10^{-14}
E_{soot} (kJ mol^{-1})	47.1

Measurements yielded fifteen values of oxidative ΔD_p at five different furnace temperatures and three inlet NO_2 mixing ratios as shown in the last three columns of Table 1. As described earlier, predictions of ΔD_p are derived corresponding to each inlet NO_2 mixing ratio and furnace temperature using eqs 1 and 2. The values of A_{soot} and E_{soot} are derived from fitting the calculated values of ΔD_p to the fifteen measurements assuming reaction order n to be 1. Table 2 reports the fitted kinetic parameters for soot oxidation using NO_2 as the oxidant under N_2 environment.

5. Discussion

As shown in Table 2, value of activation energy for soot oxidation E_{soot} is 47.1 kJ mol^{-1} assuming a reaction order of unity for soot oxidation with NO_2. This value is lower than E_{soot} values reported by prior studies. For example, Kamm et al. (*12*) derived a value of 73.1 ± 6 kJ mol^{-1} as the activation energy for soot from spark generator collected on quartz wool plugs and exposed to 1000 ppm NO_2 at 200−350 °C. They reported nonlinearity in their Arrhenius plot indicating different reaction mechanism with higher activation energy at higher temperatures. Kamm et al. (*12*) used a 3-parameter fit for just four data points at four temperatures; hence, their fitting may be biased. Choo et al. (*15*) derived an activation energy of 76.3 kJ mol^{-1} for spark discharge soot oxidation with NO_2 using the HTO-TDMA method in the temperature range 200−700 °C. However, they did not account for nonoxidative/evaporative components of ΔD_p as described earlier. In addition, Choo et al. (*15*) used an incorrect approach of deriving the value of E_{soot} from the Arrhenius plot without considering effects of varying soot oxidation rates within the furnace as function of changing temperature and NO_2 concentrations. For example, for the experimental conditions of Choo et al. (*15*), NO_2 mixing ratios are calculated to decrease by up to 27% at 700 °C inside the furnace using A_{NO_2} and E_{NO_2} values in the present study.

To compare our results with that of Choo et al. (*15*), it is necessary to reanalyze their NO_2 oxidation data in the same way as done here. Thus, the NO_2 oxidation data from Choo et al. (*15*) in their Table 1, and temperature distribution inside the furnace in their Figure 4 are chosen. For consistency, only data for three temperatures 500, 600, and 700 °C are chosen. The change in diameter ΔD_p is calculated as function of inlet NO_2 mixing ratios of 166, 386, and 552 ppm from

TABLE 1. Measured Particle Sizes and ΔD_p Values at Different Inlet NO_2 Mixing Ratios of 200, 400, and 600 ppm

set-point temperature (°C)	(a) N_2 (zero NO_2)	(b) 200 ppm NO_2	(c) 400 ppm NO_2	(d) 600 ppm NO_2	(a − b) ΔD_p 200 ppm NO_2	(a − c) ΔD_p 400 ppm NO_2	(a − d) ΔD_p 600 ppm NO_2
500	40	39	38	37	1	2	3
800	38	34	32	29	4	6	9
850	36	31	28	26	5	8	10
900	34	28	25	23	6	9	11
950	32	25	22	20	7	10	12

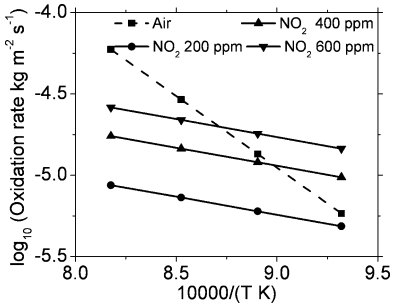

FIGURE 5. Comparison of oxidation rate of soot at different NO_2 mixing ratios in the present study and soot oxidation rate in the presence of air derived by Higgins et al. (*3*).

Table 1 in Choo et al. (*15*). NO_2 decomposition within their furnace is calculated using A_{NO_2} and E_{NO_2} values in this study. The nonoxidative component of ΔD_p measured by Choo et al. (*15*) under zero NO_2 mixing ratio is subtracted from ΔD_p measured under the presence of NO_2. Fitting is done in a manner as described in section 3 of this study using 2 parameters A_{soot} and E_{soot} to fit nine data points. Assuming a reaction order of unity, the fits to data from Choo et al. (*15*) result in an E_{soot} value of 45.7 kJ mol^{-1}. This value is significantly lower than value of 76.3 kJ mol^{-1} reported by Choo et al. (*15*) but very close to the value obtained by our study (47.1 kJ mol^{-1}). Choo et al. (*15*) overestimated the E_{soot} value by a factor of about 1.7, and this error is mainly attributed to neglecting NO_2 decomposition and error in analysis of their data. Lee et al. (*19*) investigated oxidation of Printex-U carbon black soot with NO_2 using a flow reactor system designed to simulate conditions on a diesel particulate filter. Lee et al. (*19*) derived an apparent activation energy of 60 ± 3 kJ mol^{-1} in the temperature range of 250−500 °C for oxidation with NO_2. We examined soot oxidation at a higher temperature range 500−950 °C compared to Lee et al. (*19*). This temperature range most likely represents temperature conditions during expansion stroke of diesel engines (*23*) and at the high temperature end for diesel particulate filter (DPF) regeneration. Lee et al. (*19*) and Kamm et al. (*12*) also suggested the soot reaction order of 1 with NO_2. If we let the reaction order as a third adjustable parameter in addition to A_{soot} and E_{soot} during the fitting, then a value of $n = 0.68$ and an E_{soot} value of 41.9 kJ mol^{-1} is obtained from the best fit. However, the reaction order is best determined from plots of ΔD_p versus NO_2 partial pressures in the furnace as suggested by Nienow et al. (*5*). In the present study, it is difficult to determine the reaction order with respect to NO_2, as NO_2 mixing ratios change because of thermal decomposition within the furnace.

The current activation energy for soot oxidation with NO_2 is lower as compared to soot oxidation with air. For example, Higgins et al. (*3*) found activation energy of 164 kJ mol^{-1}, while Lee et al. (*19*) derived 177 ± 1 kJ mol^{-1} for soot oxidation with O_2. Our results are consistent with other studies showing significantly lower activation energy with NO_2 oxidation as compared to O_2 (*3, 19*).

Figure 5 compares current oxidation rates derived from A_{soot} and E_{soot} values in Table 2 at different NO_2 mixing ratios, and soot oxidation rate in the presence of air derived by Higgins et al. (*3*). A density of 1800 kg m^{-3} is used for calculation of surface specific oxidation rate from diameter decrease rate following Higgins et al. (*3*). The surface specific soot oxidation rate with NO_2 is comparable to oxidation rate with air in the temperature range 800−900 °C. However, air has much higher O_2 mixing ratio (20%), while parts per million levels of NO_2 are sufficient to cause significant soot oxidation. At lower temperatures (below 500 °C), oxidation with NO_2 is expected to be higher than O_2. Experiments for lower temperature range measurement using HTO-TDMA method is a subject for further study. Further studies should also be directed toward understanding soot oxidation rates in presence of other oxidants, such as O_2 and H_2O, in addition to NO_2. These studies would help in designing improved soot emission control technologies both in-cylinder and at after-treatment systems such as the diesel particulate filter.

Acknowledgments

A part of this research was supported by the U.S. DOE's Atmospheric Systems Research Program under contract DE-AC06-76RCO 1830 at PNNL. Authors are grateful to Dr. Wayne Miller and Bill Welch to lend their instrument for this study to measure NO_2 concentration. Authors are also grateful to Drs. Kelly Higgins and Amanda Nienow for their advice in the experimental set up.

Literature Cited

(1) Neeft, J. P. A.; Makkee, M.; Moulijn, J. A. Diesel particulate emission control. *Fuel Process. Technol.* **1996**, *47* (1), 1–69.
(2) Stanmore, B. R.; Brilhac, J. R.; Gilot, P. The oxidation of soot: a review of experiments, mechanisms and models. *Carbon* **2001**, *39*, 2247–2268.
(3) Higgins, K. J.; Jung, H.; Kittelson, D. B.; Roberts, J. T.; Zachariah, M. R. Size-selected nanoparticle chemistry: Kinetics of soot oxidation. *J. Phys. Chem. A* **2002**, *106* (1), 96–103.
(4) Higgins, K. J.; Jung, H.; Kittelson, D. B.; Roberts, J. T.; Zachariah, M. R. Kinetics of diesel nanoparticle oxidation. *Environ. Sci. Technol.* **2003**, *37* (9), 1949–1954.
(5) Nienow, A. M.; Roberts, J. T.; Zachariah, M. R. Surface chemistry of nanometer-sized aerosol particles: Reactions of molecular oxygen with 30 nm soot particles as a function of oxygen partial pressure. *J. Phys. Chem. B* **2005**, *109* (12), 5561–5568.
(6) Stanmore, B. R.; Tschamber, V.; Brilhac, J. F. Oxidation of carbon by NOx, with particular reference to NO_2 and N_2O. *Fuel* **2008**, *87* (2), 131–146.
(7) Ehrburger, P. B. J.; Drouillot, Y.; Logie, V.; Gilot, P. Reactivity of Soot with Nitrogen Oxides in Exhaust Stream; *SAE Tech. Pap. Ser.* **2002**, *No 2002-01-1683.*
(8) Setiabudi, A.; Makkee, M.; Moulijn, J. A. The role of NO2 and O-2 in the accelerated combustion of soot in diesel exhaust gases. *Appl. Catal., B* **2004**, *50* (3), 185–194.
(9) Marques, R.; Darcy, P.; Da Costa, P.; Mellottee, H.; Trichard, J. M.; Djega-Mariadassou, G. Kinetics and mechanism of steady-state catalytic NO+O-2 reactions on Pt/SiO2 and Pt/CeZrO2. *J. Mol. Catal A: Chem.* **2004**, *221* (1−2), 127–136.
(10) Allansson, R. ; Andreasson, K. A.; Myers, N.; Uusimaki, A. Warren J. P. Reduction of NOx emissions of diesel engines. Eur Patent EP19980938783, 2002.
(11) Jacquot, F.; Brilhac, J. F. Soot Oxidation by O_2 and/or NO_2 in the Presence of Catalysts under Lean-Burn and Rich Atmospheres. *SAE Tech. Pap. Ser.* **2004**, *No 2004-01-1943.*
(12) Kamm, S.; Saathoff, H.; Naumann, K. H.; Möhler, O.; Schurath, U. Gasification of a soot aerosol by O_3 and NO_2: Temperature dependence of the reaction probability. *Combust. Flame* **2004**, *138* (4), 353–361.
(13) Marcuccilli, F.; Gilot, P.; Stanmore, B.; Prado, G. Experimental and theoretical study of diesel soot reactivity. *Combust. Inst., Twenty-fifth Symp. (Int.) on Combust.* **1994**, 619–626.
(14) Yezerets, A.; Currier, N. W.; Eadler, H.; Popuri, S.; Suresh, A. Quantitative Flow-Reactor Study of Diesel Soot Oxidation Process. *SAE Tech. Pap. Ser.* **2002**, No *2002-01-1684.*
(15) Choo, J.; Jung, J.; Kim, W.; Oh, H.; Kim, J.; Kim, H.; Kim, Y.; Kim, S. Oxidation characteristics of airborne carbon nanoparticles by NO_2. *Sci. Total Environ.* **2008**, *405* (1/3), 396–401.
(16) Chen, D. R.; Pui, D. Y. H.; Hummes, D.; Fissan, H.; Quant, F. R.; Sem, G. J. Design and evaluation of a nanometer aerosol differential mobility analyzer (Nano-DMA). *J. Aerosol Sci.* **1998**, *29* (5−6), 497–509.
(17) Jung, H. Size-selected nanoparticle chemistry: Kinetics of soot oxidation. Ph.D. Thesis, University of Minnesota, 2003.
(18) Shrivastava, M.; Gidwani, A.; Jung, H. Modeling oxidation of soot particles within a laminar aerosol flow reactor using computational fluid dynamics. *Aerosol Sci. Technol.* **2009**, *43* (12), 1218–1229.
(19) Lee, J. H.; Lee, H.-S.; Song, S.; Chun, K. M. Experimental Investigation of Soot Oxidation Characteristic with NO_2 and O_2

using a Flow Reactor Simulating DPF. *SAE Tech. Pap. Ser.* **2007**, *No 2007-01-1270*.
(20) Park, J.; Giles, N. D.; Moore, J.; Lin, M. C. A comprehensive kinetic study of thermal reduction of NO_2 by H-2. *J. Phys. Chem. A* **1998**, *102* (49), 10099–10105.
(21) Muckenhuber, H.; Grothe, H. The heterogeneous reaction between soot and NO_2 at elevated temperature. *Carbon* **2006**, *44* (3), 546–559.
(22) Muckenhuber, H.; Grothe, H. A DRIFTS study of the heterogeneous reaction of NO_2 with carbonaceous materials at elevated temperature. *Carbon* **2007**, *45* (2), 321–329.
(23) Ma, H.; Jung, H.; Kittelson, D. B. Investigation of diesel nanoparticle nucleation mechanisms. *Aerosol Sci. Technol.* **2008**, *42* (5), 335–342.

ES903672Y